ChemComm

COMMUNICATION

View Article Online
View Journal | View Issue

Cite this: *Chem. Commun.*, 2026, **62**, 616

Received 25th August 2025,
Accepted 27th November 2025

DOI: 10.1039/d5cc04879f

rsc.li/chemcomm

Catalytic dinitrogen silylation by tris(pyrazolyl)borate-supported titanium complexes

Chenrui Liu,†[a] Ling-Ya Peng,†[b] Yumeng Chen,†[a] Jingyi An,[a] Zhaoxin Li,[a] Wenshuang Huang,[a] Ganglong Cui *[ac] and Shaowei Hu *[a]

Titanium dinitrogen complexes supported by tris(pyrazolyl)borate and alkoxide/aryloxide ligands catalyse N_2 silylation. Titanium silylimide and disilylamide model complexes represent the first well-defined group IV imide/amide catalysts for N_2 reduction. Silylamine release and regeneration of the dinitrogen complex highlight the potential of early transition metals for N_2 catalysis.

The activation and transformation of chemically inert dinitrogen (N_2) is a fundamental challenge with significant implications for human society. In nature, certain microorganisms convert N_2 to ammonia under ambient conditions using nitrogenases.[1] In contrast, the industrial Haber–Bosch process, which converts N_2 and H_2 into NH_3, requires high temperatures and pressures, making it highly energy-intensive.[2]

To better understand nitrogen fixation and develop catalysts for milder conditions, various studies on artificial N_2 fixation with transition metal complexes have been conducted.[3] Several complexes have been developed to catalyse the conversion of N_2 to NH_3 in the presence of electron and proton sources.[4] Alternatively, the reduction of N_2 to silylamines catalysed by transition metal complexes can be achieved in the presence of reducing and silylating agents, broadening the approaches to functionalizing dinitrogen.[5] While significant progress has been made with middle and late transition metal dinitrogen complexes, well-defined group IV metal complexes capable of catalysing N_2 conversion to ammonia or silylamines remain scarce.[6] Furthermore, group IV metal imide or amide catalysts have not yet been reported.[7] Here, we present a series of titanium dinitrogen complexes bearing tris(pyrazolyl)borate (Tp) and alkoxide or aryloxide ligands that mediate the catalytic reduction of N_2 to silylamines. Additionally, separately synthesized titanium silylimide and disilylamide complexes represent unprecedented well-defined group IV imide/amide species capable of catalyzing N_2 reduction. Key transformation steps, such as the release of silylamine and regeneration of the titanium dinitrogen complex, have also been elucidated.

The tris(pyrazolyl)borates (Tp) are attractive ligands for catalysts in various transformations and generally considered as formal analogues of the cyclopentadienyl ligand, owing to their similar charge, number of electrons donated and facial coordination geometry.[8] Tp-ligated titanium alkyl and chloride complexes have shown notable activity in olefin polymerization,[8,9] highlighting their ability to stabilize reactive titanium centres. Motivated by these properties, we explore Tp-supported titanium complexes as potential catalysts for N_2 fixation. In view of the fact that transition metal complexes featuring Tp ligands capable of activating dinitrogen are relatively rare,[10] the investigation of Tp-supported group IV metal complexes for dinitrogen fixation is obviously of great interest and importance.

A Tp* (Tp* = HB(3,5-Me_2-pyrazolyl)$_3$) supported titanium chloride complex Tp*$TiCl_2$(THF) could be conveniently prepared through the reaction of $TiCl_3(THF)_3$ and Tp*K (Scheme 1A). Building on our recent discoveries in vanadium and molybdenum catalysis for dinitrogen reduction, where bulky alkoxide or aryloxide ligands were crucial in stabilizing complexes and enhancing catalytic activity,[11] we introduced similar groups into the titanium complexes. Treatment of Tp*$TiCl_2$(THF) with one equivalent of lithium aryloxide or alkoxide in toluene afforded Tp*Ti(L)Cl (L = $OC_6H_3Me_2$-2,6, **1a**, 53%; L = $OC_6H_3{}^{i}Pr_2$-2,6, **1b**, 56%; L = $OC_6H_3{}^{t}Bu$-2,6, **1c**, 64%; L = O^{t}Bu, **1d**, 63%). Complexes **1a**, **1b**, and **1d** feature a coordinated THF ligand and adopt similar distorted octahedral geometries, whereas steric congestion imposed by the bulky 2,6-di-*tert*-butylphenoxide ligand in **1c** precludes THF coordination, resulting in a slightly distorted square pyramidal geometry (τ = 0.36, see the SI).

Reduction of **1a** with two equivalents of KC_8 in THF at room temperature under a N_2 atmosphere afforded a dinitrogen-

[a] *College of Chemistry, Beijing Normal University, No. 19, Xin-wai street, Beijing 100875, P. R. China. E-mail: shu@bnu.edu.cn*
[b] *School of Chemistry and Chemical Engineering, Shaanxi Normal University, Xi'an 710119, China*
[c] *Key Laboratory of Theoretical and Computational Photochemistry, Ministry of Education, College of Chemistry, Beijing Normal University, Beijing 100875, P. R. China. E-mail: ganglong.cui@bnu.edu.cn*
† These authors contributed equally to this work.

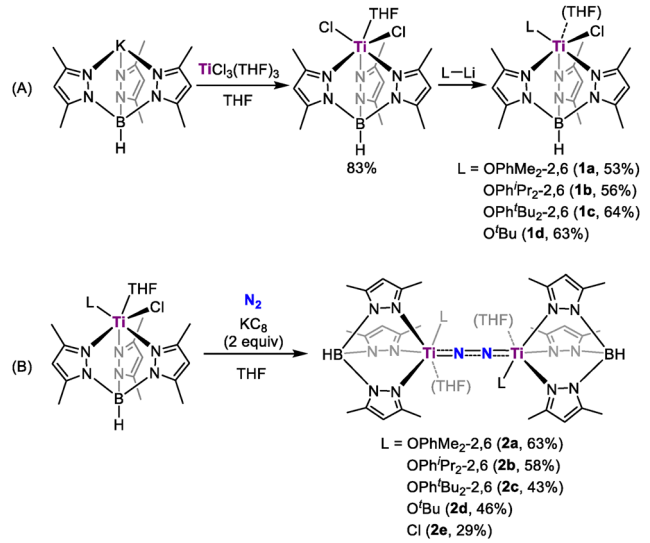

Scheme 1 Synthesis of titanium chloride complexes (A) and their reduction to dinitrogen complexes (B)

bridged dititanium complex $[Tp^*Ti(OC_6H_3Me_2\text{-}2,6)]_2(\mu\text{-}\eta^1\text{:}\eta^1\text{-}N_2)(THF)_2$ (**2a**) in 63% yield as dark green crystals (Scheme 1B). Complex **2a** is stable both in the solid-state or in solution at room temperature. X-ray diffraction study revealed that the dinitrogen ligand is bonded to two Ti atoms in an end-on bridged manner, with each Ti atom also coordinated by a Tp* ligand, a THF molecule and a 2,6-dimethylphenoxide ligand (Fig. 1). **2a** has a nearly linear Ti1–N1–N2–Ti2 topology, with Ti1–N1–N2 and Ti2–N2–N1 angles of 174.0(2)° and 173.2(1)°. The N–N bond length (1.237(2) Å) is significantly elongated compared to free N_2 (1.098 Å), and slightly shorter than that of $[(Me_2N)C(N^iPr)]_4Ti_2(\mu\text{-}N_2)$ (1.28(1) Å)[12] and $\{[(Me_3Si)_2NC\text{-}(NC_6H_{11})_2]_4Ti\}_2(\mu\text{-}N_2)$ (1.278(3) Å),[13] suggesting strong activation of N_2. The Ti–N bond distances (Ti1–N1: 1.805(2) Å; Ti2–N2: 1.802(2) Å) are longer than $Ti\text{–}N_{imido}$ (1.689(2) Å) in [(nacnac)Ti = NH(Ntol$_2$)] (nacnac = $[(2,6\text{-}^iPr_2C_6H_3)NC(CH_3)]_2CH$, tol = 4-$CH_3C_6H_4$),[14] but shorter than the $Ti\text{–}N_{amido}$ (1.932(4) Å) bond distances in $[(Me_3Si)_2C_5H_3]_2Ti(NH_2)$,[15] indicating the existence of σ- and π-bonding in the Ti–N bonds. The ^{15}N NMR spectrum of the isotopically labelled complex **2a-^{15}N**, prepared from the reaction of **1a** with KC_8 under $^{15}N_2$, displays a singlet at δ 48.2 ppm. This substantial upfield shift from the value of 114.7 ppm reported for $[(OO)Ti(C_5H_5N)]_2(\mu\text{-}\eta^1\text{:}\eta^1\text{-}N_2)$ (OO = (1,4-$(OC_6H_4Me^tBu)_2C_6H_4$))[16] is indicative of increased electron density and a reduced bond order of the N–N unit, demonstrating a much higher degree of N_2 activation in **2a**.

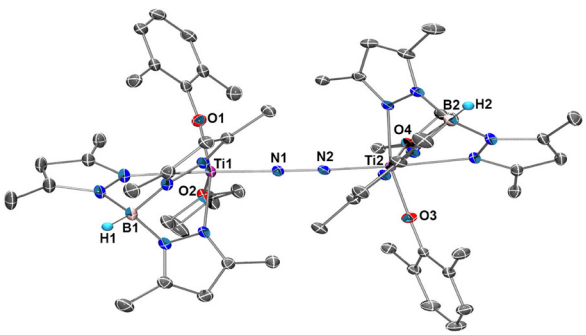

Fig. 1 Molecular structure in the solid-state of **2a** with thermal ellipsoids drawn at 30% probability. Hydrogen atoms were omitted for clarity.

The computed Ti–N Mayer bond orders of 1.55 further support this bond interaction. The X-ray photoelectron spectroscopy (XPS) analysis of **2a** reveals a binding energy of 458.06 eV (Fig. S16), which indicates that the oxidation states of the metal centres tend to be Ti(IV).[13] The UV-vis spectroscopic studies of **2a** exhibited absorption at 336 nm. The Raman spectrum of solid **2a** displayed a peak at 1336 cm^{-1}, which shifted to 1307 cm^{-1} in **2a-^{15}N**. This unusual low ν(N–N) stretching vibration indicates a significant reduction of N–N bond order and is consistent with the computational analysis. Solid-state magnetization measurements (SQUID) for **2a** showed no paramagnetic signal, reflecting the diamagnetic nature of the complex.

The electronic structure of **2a** was explored through theoretical calculations using the B3LYP/def2-SVP method. Complex **2a** behaves as a closed-shell species. Analysis of the frontier orbitals reveals two π-orbital interactions between the π* orbitals of dinitrogen and d_{xy} (d_{xz}) orbitals of two titanium atoms (Fig. S29). In the HOMO, the main contributions come from the two titanium centres (20.3% and 20.2%) and dinitrogen (36.5%). While the HOMO−1 consists primarily of the 3d orbitals of titanium (26.2% and 26.1%) and the π* orbitals (37.8%) of dinitrogen. This suggests a double-bond character between each titanium and nitrogen atom. Natural bond orbital analysis further supports this observation (see the SI).

Other Tp* ligated titanium dinitrogen complexes were prepared using similar approaches. Complexes $[Tp^*Ti(OC_6H_3Me_2\text{-}2,6)]_2(\mu\text{-}\eta^1\text{:}\eta^1\text{-}N_2)(THF)_2$ (L = $OC_6H_3{}^iPr_2$-2,6, **2b**; L = O^{t}Bu, **2d**; L = Cl, **2e**) were isolated in a yield of 58%, 46% and 29%, respectively. X-ray diffraction analysis confirmed that the structures of **2b**, **2d**, and **2e** are similar to that of **2a** (see the SI). In contrast, the 2,6-di-*tert*-butylphenoxide ligated titanium dinitrogen complex $[Tp^*Ti(OC_6H_3{}^tBu_2\text{-}2,6)]_2(\mu\text{-}\eta^1\text{:}\eta^1\text{-}N_2)$ (**2c**) was prepared as a THF-free titanium dinitrogen complex, attributed to the increased steric hindrance around the metal centre (Fig. S24).

With a series of titanium dinitrogen complexes in hand, we have explored the catalytic reductions of dinitrogen into ammonia. However, an only slightly greater-than-stoichiometric amount of NH_3 (2.7 ± 0.1) was detected when **2a** was utilized as a catalyst with $[H(Et_2O)_2][BAr^F{}_4]$ (Ar^F = (3,5-$(CF_3)_2C_6H_3$)) as the acid and KC_8 as the reductant (see the SI). Alternatively, we investigated the capabilities of titanium complexes in the catalytic silylation of dinitrogen using silicon and electron equivalents. The initial investigation of N_2 reduction performance employed Me_3SiCl as the silicon source and KC_8 as the electron source. The generated tris(trimethylsilyl)amine was hydrolyzed with HCl, and the resulting NH_4Cl was quantified by the indophenol method (Table 1).

The turnover number (TON) was calculated based on the amount of silylamine produced per Ti center. To ensure accurate quantification, the products from the same catalytic run, namely $N(SiMe_3)_3$ and $NH_4{}^+$ (from hydrolysis), were analysed *via* independent methods (^{1}H NMR and GC-MS for the silylamine,

Table 1 Catalytic N_2 reduction to silylamine by Ti complexes

N_2 + R_3SiCl + KC_8 —[Ti]→ $N(SiMe_3)_3$ —H^+→ NH_4^+

Entry	Cat.	Reductant	R_3SiCl[a]	Solvent	TON[b]	Yield[c]/%
1	**2a**	KC_8 (100)	Me_3SiCl (100)	THF	5.9 ± 0.9	35
2	**2b**	KC_8 (100)	Me_3SiCl (100)	THF	6.0 ± 0.3	36
3	**2c**	KC_8 (100)	Me_3SiCl (100)	THF	5.9 ± 0.2	35
4	**2d**	KC_8 (100)	Me_3SiCl (100)	THF	5.4 ± 1.2	32
5	**2e**	KC_8 (100)	Me_3SiCl (100)	THF	5.1 ± 0.6	31
6	–	KC_8 (100)	Me_3SiCl (100)	THF	0.1 ± 0	0.2
7	**3a**	KC_8 (100)	Me_3SiCl (100)	THF	5.9 ± 0.6	35
8	**4a**	KC_8 (100)	Me_3SiCl (100)	THF	7.5 ± 0.7	45

Reactions were performed at −40 °C. [a] Stoichiometric quantities of Me_3SiCl and reductant. [b] TON = equiv. of [$N(SiMe_3)_3$]/equiv of [Ti], and represents the average of ≥2 independent runs. [c] Yield = 3 × NH_4^+/reductant.

and the indophenol method for ammonia), all of which showed consistent results. Under conditions of 100 equiv. of Me_3SiCl and 100 equiv. of KC_8 in THF at room temperature, both the dinitrogen complexes (**2a–e**) and their precursors (Tp*$TiCl_2$(THF) and **1a–d**) produced only a small amount of $N(SiMe_3)_3$ (1.9–4.1 equiv.) with yields spanning a range from 6% to 18% (Table S2). The catalytic reaction generated side products including $Me_3SiSiMe_3$ (13% yield) and $Me_3SiOC_4H_9$ (~1% yield), implicating trimethylsilyl radicals ($Me_3Si^•$) in pathways involving dimerization and reaction with the THF solvent.[17] As lower temperature can suppress side reactions,[11b] we conducted the catalysis with **2a** at −40 °C, resulting in an increased production of silylamine (5.9 ± 0.9 equiv.) and an improved overall yield of 35% (entry 1). Similarly, **2b** produced up to 6.0 ± 0.3 equiv. of $N(SiMe_3)_3$ with a yield of 36%. Besides, we have investigated the effectiveness of various reducing agents, including Li, Na, K, and KC_8, finding that KC_8 was the most effective (5.9 *vs.* 0.5–5.8 equiv., Table S6). To trace the nitrogen source, catalysis was conducted with complex **2a-^{15}N** under a $^{15}N_2$ atmosphere. After acidic work-up, $^{15}NH_4^+$ was detected by ^{1}H NMR spectroscopy (Fig. S15), unambiguously verifying dinitrogen gas as the nitrogen source.

Additionally, we explored the reactions in toluene, THF, DME, and Et_2O, determining that the conditions in THF exhibited better conversion than those in other solvents (5.9 *vs.* 0.3–5.5, Table S4). The catalysis was further explored using other sterically hindered silicon reagents. However, lower amounts of silylamines were detected with $^iPr_3SiCl$ and chlorodimethylvinylsilane ($Me_2(CH_2CH)SiCl$) (Table S5).

To gain more information about the catalytic process, stoichiometric reactions of **1a** with Me_3SiCl and KC_8 were performed, but no intermediate complex was isolated, likely due to its high reactivity under the reaction conditions. On the other hand, we have also attempted to synthesize the titanium silylimide model complex by adding Me_3SiN_3 to a toluene solution of **2a**. The reaction afforded complex Tp*Ti = NSiMe_3($OC_6H_3Me_2$-2,6)(THF) (**3a**) in 59% yield, accompanied by the extrusion of N_2 (Scheme 2A). X-ray diffraction of **3a** shows a six-coordinate mononuclear framework with a silylimido ligand, an aryloxide ligand, a coordinated THF molecule, and a Tp* ligand, adopting a slightly distorted octahedral geometry

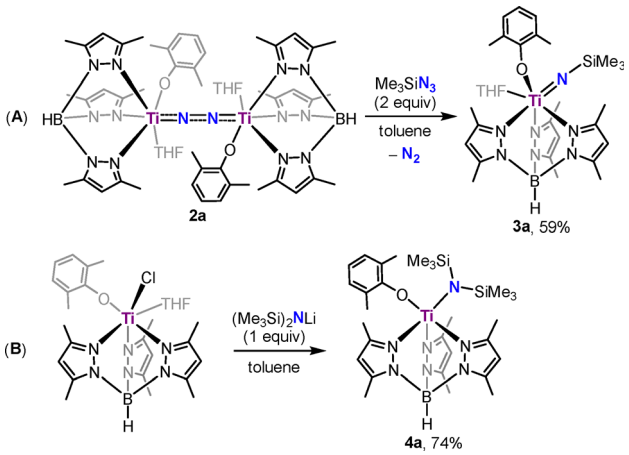

Scheme 2 Synthesis of silylimide (**3a**, A) and disilylamide (**4a**, B) complexes.

(Fig. 2). The silylimido ligand is coordinated to the Ti atom in a near-linear manner (Ti1–N1–Si1: 178.3(1)°). The Ti–N distance in **3a** (Ti1–N1: 1.725(2) Å) is longer than that of reported Ti–$N_{nitrido}$ bonds (1.660(2) Å)[18] and shorter than that of Ti–N_{amide} bonds (1.929(3) Å).[19]

Separately, reaction of **1a** with lithium bis(trimethylsilyl)amide at room temperature afforded the titanium bis(trimethylsilyl)amide complex Tp*Ti[$N(SiMe_3)_2$]($OC_6H_3Me_2$-2,6)(THF) (**4a**) in 74% yield as orange crystals, structurally confirmed by X-ray diffraction (Scheme 2B, for details see the SI).

Treatment of **3a** with one equivalent of KC_8 and Me_3SiCl at −40 °C led to the release of $N(SiMe_3)_3$ in 28% yield, with recovery of unreacted **3a**. In contrast, **4a** under the same conditions afforded $N(SiMe_3)_3$ in 68% yield along with regeneration of the titanium dinitrogen complex **2a** (33% yield), suggesting that **3a** might first form **4a** before converting to **2a**. Under catalytic conditions (100 equiv. of KC_8 and Me_3SiCl at −40 °C under N_2), **3a** and **4a** served as active catalysts for dinitrogen silylation (Table 1, entries 7 and 8). Notably, **4a** exhibited the highest TON of 7.5 ± 0.7 with a yield of 45%.

Transition metal dinitrogen complexes are widely employed as catalysts for synthesizing ammonia and silylamines from N_2, with imide and amide species recognized as key intermediates. However, effective imide and amide complex catalysts for N_2 reduction are rare. While molybdenum and iron imide/amide

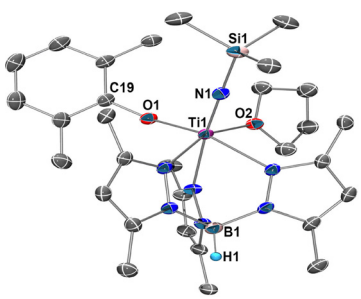

Fig. 2 Molecular structure in the solid-state of **3a** with thermal ellipsoids drawn at 30% probability. Hydrogen atoms were omitted for clarity.

complexes show notable silylation activity,[7] group IV analogues remain unreported. Here titanium silylimide and disilylamide complexes provide the first such examples, displaying catalytic performance comparable to that of dinitrogen complexes.

Notably, the disilylamide complex liberated $N(SiMe_3)_3$ and regenerated the titanium dinitrogen complex in the present of KC_8 and Me_3SiCl, modelling the late-stage cycle. These results suggest a plausible mechanism where reductive silylation of the dititanium dinitrogen complex affords silylimide and disilylamide intermediates, which release $N(SiMe_3)_3$ and regenerate dinitrogen complexes upon further silylation. A pathway where $N_2(SiMe_3)_4$ is released and subsequently converted to $N(SiMe_3)_3$ cannot be excluded.[6a,b,20]

In summary, this work demonstrates catalytic N_2 silylation using Tp-supported titanium complexes and reports the first well-defined group IV silylimide/disilylamide catalysts for this reaction. The observed reactivity, particularly the disilylamide's ability to liberate silylamine and close the catalytic cycle by regenerating the dinitrogen complex, supports a plausible pathway involving silylation of bimetallic dinitrogen-bridged titanium species. These findings establish Tp-supported titanium complexes as a unique platform for dinitrogen functionalization, underscoring the broader potential of early transition metals in catalytic N_2 reduction.

This work was supported by the National Natural Science Foundation of China (22371017), Startup Funding from Beijing Normal University (312232110), the Young Thousand Talents Program (110532107) and the Fundamental Research Funds for the Central Universities. We thank Prof. Haoling Sun (Beijing Normal University) for SQUID measurements, and Prof. Zhi Li and Ms Gangmei Li (Beijing Normal University) for the help with XPS analysis.

Conflicts of interest

There are no conflicts to declare.

Data availability

The data supporting this article have been included as part of the supplementary information (SI). Supplementary information: synthetic procedures, NMR, UV-Vis and Raman spectra, crystallographic data, and computational details. See DOI: https://doi.org/10.1039/d5cc04879f.

CCDC 2331148 (**1a**), 2331149 (**1b**), 2350473 (**1c**), 2216825 (**1d**), 2310979 (**2a**), 2311060 (**2b**), 2350469 (**2c**), 2311244 (**2d**), 2312824 (**2e**), 2334087 (**3a**) and 2331239 (**4a**) contain the supplementary crystallographic data for this paper.[21a–k]

Notes and references

1 (*a*) B. M. Hoffman, D. Lukoyanov, Z.-Y. Yang, D. R. Dean and L. C. Seefeldt, *Chem. Rev.*, 2014, **114**, 4041–4062; (*b*) O. Einsle and D. C. Rees, *Chem. Rev.*, 2020, **120**, 4969–5004.
2 J. W. Erisman, M. A. Sutton, J. Galloway, Z. Klimont and W. Winiwarter, *Nat. Geosci.*, 2008, **1**, 636–639.
3 (*a*) S. Kim, F. Loose and P. J. Chirik, *Chem. Rev.*, 2020, **120**, 5637–5681; (*b*) D. Singh, W. R. Buratto, J. F. Torres and L. J. Murray, *Chem. Rev.*, 2020, **120**, 5517–5581; (*c*) S. J. K. Forrest, B. Schluschaß, E. Y. Yuzik-Klimova and S. Schneider, *Chem. Rev.*, 2021, **121**, 6522–6587; (*d*) Z.-J. Lv, J. Wei, W.-X. Zhang, P. Chen, D. Deng, Z.-J. Shi and Z. Xi, *Natl. Sci. Rev.*, 2020, **7**, 1564–1583.
4 (*a*) M. J. Chalkley, M. W. Drover and J. C. Peters, *Chem. Rev.*, 2020, **120**, 5582–5636; (*b*) Y. Tanabe and Y. Nishibayashi, *Coord. Chem. Rev.*, 2022, **472**, 214783.
5 Y. Tanabe and Y. Nishibayashi, *Coord. Chem. Rev.*, 2019, **389**, 73–93.
6 (*a*) L. R. Doyle, A. J. Wooles, L. C. Jenkins, F. Tuna, E. J. L. McInnes and S. T. Liddle, *Angew. Chem., Int. Ed.*, 2018, **57**, 6314–6318; (*b*) A. Wong, F. Y. T. Lam, M. Hernandez, J. Lara, T. M. Trinh, R. P. Kelly, T. Ochiai, G. Rao, R. D. Britt, N. Kaltsoyannis and P. L. Arnold, *Chem Catal.*, 2024, **4**, 100964; (*c*) P. Ghana, F. D. van Krüchten, T. P. Spaniol, J. van Leusen, P. Kögerler and J. Okuda, *Chem. Commun.*, 2019, **55**, 3231–3234; (*d*) M. Mori, *J. Organomet. Chem.*, 2004, **689**, 4210–4227.
7 (*a*) Q. Liao, N. Saffon-Merceron and N. Mézailles, *Angew. Chem., Int. Ed.*, 2014, **53**, 14206–14210; (*b*) Q. Liao, N. Saffon-Merceron and N. Mézailles, *ACS Catal.*, 2015, **5**, 6902–6906; (*c*) R. Araake, K. Sakadani, M. Tada, Y. Sakai and Y. Ohki, *J. Am. Chem. Soc.*, 2017, **139**, 5596–5606.
8 S. Trofimenko, *Chem. Rev.*, 1993, **93**, 943–980.
9 (*a*) L. E. Manzer, *J. Organomet. Chem.*, 1975, **102**, 167–174; (*b*) S. Murtuza, O. L. Casagrande and R. F. Jordan, *Organometallics*, 2002, **21**, 1882–1890; (*c*) K. Itagaki, K. Kakinuki, S. Katao, T. Khamnaen, M. Fujiki, K. Nomura and S. Hasumi, *Organometallics*, 2009, **28**, 1942–1949.
10 (*a*) D. C. Cummins, G. P. A. Yap and K. H. Theopold, *Eur. J. Inorg. Chem.*, 2016, 2349–2356; (*b*) S. Zhang, H. Fallah, E. J. Gardner, S. Kundu, J. A. Bertke, T. R. Cundari and T. H. Warren, *Angew. Chem., Int. Ed.*, 2016, **55**, 9927–9931; (*c*) A. Reinholdt, D. Pividori, A. L. Laughlin, I. M. DiMucci, S. N. MacMillan, M. G. Jafari, M. R. Gau, P. J. Carroll, J. Krzystek, A. Ozarowski, J. Telser, K. M. Lancaster, K. Meyer and D. J. Mindiola, *Inorg. Chem.*, 2020, **59**, 17834–17850.
11 (*a*) W. Huang, L.-Y. Peng, J. Zhang, C. Liu, G. Song, J.-H. Su, W.-H. Fang, G. Cui and S. Hu, *J. Am. Chem. Soc.*, 2023, **145**, 811–821; (*b*) Z. Li, C. Liu, J. An, X. Wang and S. Hu, *ACS Catal.*, 2024, **14**, 6558–6564.
12 S. M. Mullins, A. P. Duncan, R. G. Bergman and J. Arnold, *Inorg. Chem.*, 2001, **40**, 6952–6963.
13 B. Wu, R. Feng, Z.-B. Yin, H. Yan, X. Wang, G.-X. Wang, J. Wei and Z. Xi, *Sci. China: Chem.*, 2023, **66**, 755–759.
14 B. L. Tran, M. P. Washington, D. A. Henckel, X. Gao, H. Park, M. Pink and D. J. Mindiola, *Chem. Commun.*, 2012, **48**, 1529–1531.
15 C. D. Sofield, M. D. Walter and R. A. Andersen, *Acta Crystallogr., Sect. C: Cryst. Struct. Commun.*, 2004, **60**, m465–m466.
16 T. Kurogi, Y. Ishida and H. Kawaguchi, *Chem. Commun.*, 2013, **49**, 11755–11757.
17 (*a*) J. H. Sharp and M. C. R. Symons, *J. Chem. Soc. A*, 1970, 3084–3087, DOI: 10.1039/J19700003084; (*b*) L. E. Gusel'nikov, Y. P. Polyakov, E. A. Volnina and N. S. Nametkin, *J. Organomet. Chem.*, 1985, **292**, 189–203.
18 M. E. Carroll, B. Pinter, P. J. Carroll and D. J. Mindiola, *J. Am. Chem. Soc.*, 2015, **137**, 8884–8887.
19 B. C. Bailey, F. Basuli, J. C. Huffman and D. J. Mindiola, *Organometallics*, 2006, **25**, 2725–2728.
20 R. Feng, Y. Jiang, X. Shi, X. Wang, W. Chen, F. Xie, J. Su, J. Wei, S. Ye and Z. Xi, *CCS Chem.*, 2023, **5**, 2473–2481.
21 (*a*) CCDC 2331148: Experimental Crystal Structure Determination, 2025, DOI: 10.5517/ccdc.csd.cc2j7rbw; (*b*) CCDC 2331149: Experimental Crystal Structure Determination, 2025, DOI: 10.5517/ccdc.csd.cc2j7rcx; (*c*) CCDC 2350473: Experimental Crystal Structure Determination, 2025, DOI: 10.5517/ccdc.csd.cc2jwvq0; (*d*) CCDC 2216825: Experimental Crystal Structure Determination, 2025, DOI: 10.5517/ccdc.csd.cc2ddsh3; (*e*) CCDC 2310979: Experimental Crystal Structure Determination, 2025, DOI: 10.5517/ccdc.csd.cc2hkrqk; (*f*) CCDC 2311060: Experimental Crystal Structure Determination, 2025, DOI: 10.5517/ccdc.csd.cc2hkvb8; (*g*) CCDC 2350469: Experimental Crystal Structure Determination, 2025, DOI: 10.5517/ccdc.csd.cc2jwvlw; (*h*) CCDC 2311244: Experimental Crystal Structure Determination, 2025, DOI: 10.5517/ccdc.csd.cc2hl18f; (*i*) CCDC 2312824: Experimental Crystal Structure Determination, 2025, DOI: 10.5517/ccdc.csd.cc2hmp72; (*j*) CCDC 2334087: Experimental Crystal Structure Determination, 2025, DOI: 10.5517/ccdc.csd.cc2jbt4v; (*k*) CCDC 2331239: Experimental Crystal Structure Determination, 2025, DOI: 10.5517/ccdc.csd.cc2j7v8x.